Toward Variable-Friction Catheters Using Ultrasonic Lubrication

Atalla, Mostafa A.; Tuijp, Jeroen J.; Wiertlewski, Michael; Sakes, Aimee

DOI
10.1109/TMRB.2024.3464672

Publication date
2024

Document Version
Final published version

Published in
IEEE Transactions on Medical Robotics and Bionics

Toward Variable-Friction Catheters Using Ultrasonic Lubrication

Mostafa A. Atalla, *Graduate Student Member, IEEE*, Jeroen J. Tuijp, Michaël Wiertlewski, *Member, IEEE*, and Aimée Sakes

***Abstract*—Minimally invasive endovascular procedures use catheters that are guided through blood vessels to perform interventions, resulting in an inevitable frictional interaction between the catheter and the vessel walls. While this friction enhances stability during the intervention, it poses a risk of damaging the inner layer of the blood vessel wall during navigation, leading to post-operative complications including infectious diseases and thrombus formation. To mitigate the risk of adverse complications, we propose a new concept of a variable-friction catheter capable of transitioning from low friction during navigation to high friction for increased stability while performing the intervention. This variable-friction catheter leverages ultrasonic lubrication to actively control the frictional forces experienced by the catheter during the procedure. In this paper, we demonstrate a proof-of-concept for a friction control module, a pivotal component of the proposed catheter design. Our experiments demonstrate that the prototype effectively reduce friction by up to 11% and 60%, on average, on soft and rigid surfaces, representing its potential performance on healthy and calcified tissue, respectively. This result underscores the feasibility of the design and its potential to improve the safety and efficacy of minimally invasive endovascular procedures.**

***Index Terms*—Catheter technology, ultrasonic lubrication, friction modulation, friction control.**

I. Introduction

Over the past few decades, minimally-invasive endovascular interventions superseded conventional open heart surgeries, leading to shorter recovery times and lower infection rates. In a typical endovascular catheterization procedure, the interventionist inserts a catheter in the radial or femoral artery and navigates it through the arteries to the heart, where the intervention is performed. In order to safely reach the heart, catheters (and guidewires) used during these procedures need to easily follow the curves in the vascular system, while creating as little friction as possible with the blood vessel wall. When these devices exhibit high friction, their insertion risks damaging the mucous membranes or the intima of the blood vessels, which may lead to infectious diseases or thrombus formation [1], [2], [3]. While low friction is beneficial to avoid damage to the membranes and blood vessel wall, it complicates holding a specific location in open spaces, such as inside the heart. This problem is particularly true when high forces need to be applied, such as when cutting or puncturing tissues. This suggests the need for an active friction management technique that can regulate the frictional properties of catheters depending on the phase of the catheterization procedure; for instance, having low friction while navigating through the vasculature and switching to a high friction state while executing the surgical task.

Friction management strategies in catheterization procedures are typically passive. Current practices involve direct application of lubricants, aiming to reduce the risk of tissue damage during sliding [4], [5], [6], [7]. Another approach uses specially coated self-lubricating instruments, like hydrophilic catheters, which become lubricated when into contact with a wet surface [8], [9]. The first approach, involving direct application of lubricants, faces a limitation: the effectiveness of the lubricant is short-lived and easily wiped off during sliding. Consequently, its utility is restricted to relatively short distances [5]. The second approach, centred around specialized coatings, like hydrophilic surfaces, is procedure-specific, primarily applicable to procedures involving water-based fluid contact such as urology, and lacks versatility for broader catheterization applications. Furthermore, the inability to switch between high and low friction levels in both methods poses challenges in instrument stabilization. The limitations of the existing practices evidently suggest the need for an active friction modulation strategy. A strategy that allows instruments to transition between high and low friction states in real-time based on the different stages of the intervention.

We propose a catheter design in which friction can be programmed. The catheter is built around several discrete modules each of which can provide friction modulation using ultrasonic vibration along the shaft of the catheter. In this paper, we present a proof-of-concept of the friction control modules, alongside results from simulation and experimental validation, including sliding friction experiments.

II. Working Principle and Design

A. Ultrasonic Lubrication

When two objects come into contact and undergo relative sliding, friction arises as a consequence of the interaction between a finite number of microscopic surface roughness asperities, as illustrated in Fig. 1(a). These asperities form junctions with the opposite surface that collectively form a *real* area of contact, which is significantly smaller than the apparent area of contact. Consequently, a substantial portion of the apparent contact area remains disengaged, entrapping fluid from the surrounding medium and forming a thin film of fluid, known as a squeeze film, along the interface.

When transverse ultrasonic vibrations are applied to one of the objects in contact, the fluid trapped between the asperities undergoes non-linear compression, resulting in a net positive overpressure in

Received 19 January 2024; revised 8 June 2024; accepted 25 July 2024. Date of publication 20 September 2024; date of current version 12 November 2024. This article was recommended for publication by Associate Editor A. Kuntz and Editor P. Dario upon evaluation of the reviewers' comments. This work was supported by a TU Delft Cohesion Grant. *(Michaël Wiertlewski and Aimée Sakes contributed equally to this work.) (Corresponding author: Mostafa A. Atalla.)*

Mostafa A. Atalla is with the Department of BioMechanical Engineering, Faculty of Mechanical Engineering, and the Department of Cognitive Robotics, Faculty of Mechanical Engineering, Delft University of Technology, 2628 CD Delft, The Netherlands (e-mail: m.a.a.atalla@tudelft.nl).

Jeroen J. Tuijp and Aimée Sakes are with the Department of BioMechanical Engineering, Faculty of Mechanical Engineering, Delft University of Technology, 2628 CD Delft, The Netherlands.

Michaël Wiertlewski is with the Department of Cognitive Robotics, Faculty of Mechanical Engineering, Delft University of Technology, 2628 CD Delft, The Netherlands.

Digital Object Identifier 10.1109/TMRB.2024.3464672

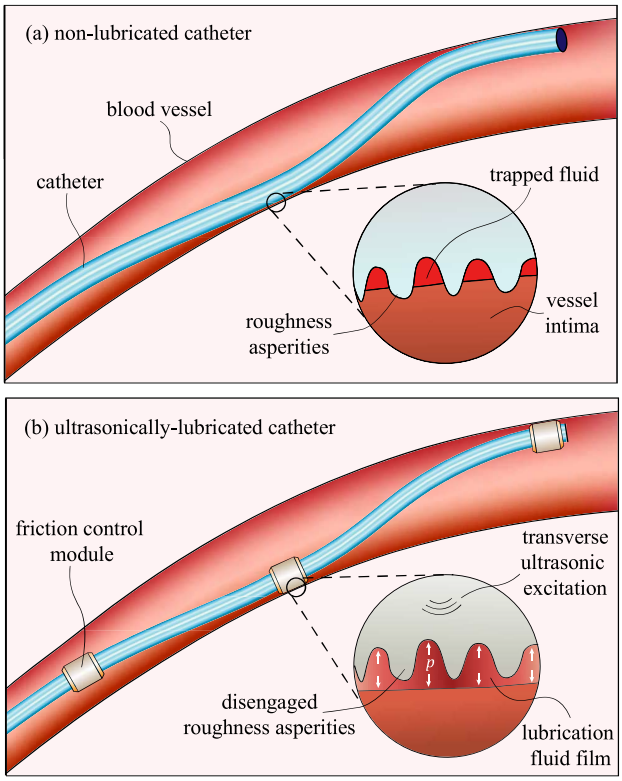

Fig. 1. Ultrasonically-lubricated catheters. (a) conventional catheter in a blood vessel where contact occurs at multiple points along its lumen. The magnified view shows the asperities contact at a microscopic scale, which results in complications when the catheter slides relative to the vessel. (b) the proposed variable-friction catheter with integrated friction control modules along its shaft. The magnified view shows the interface of the friction control module surface and the vessel, which creates an active lubrication fluid film resulting in a disengagement of the asperities leading to a smooth and safe sliding motion.

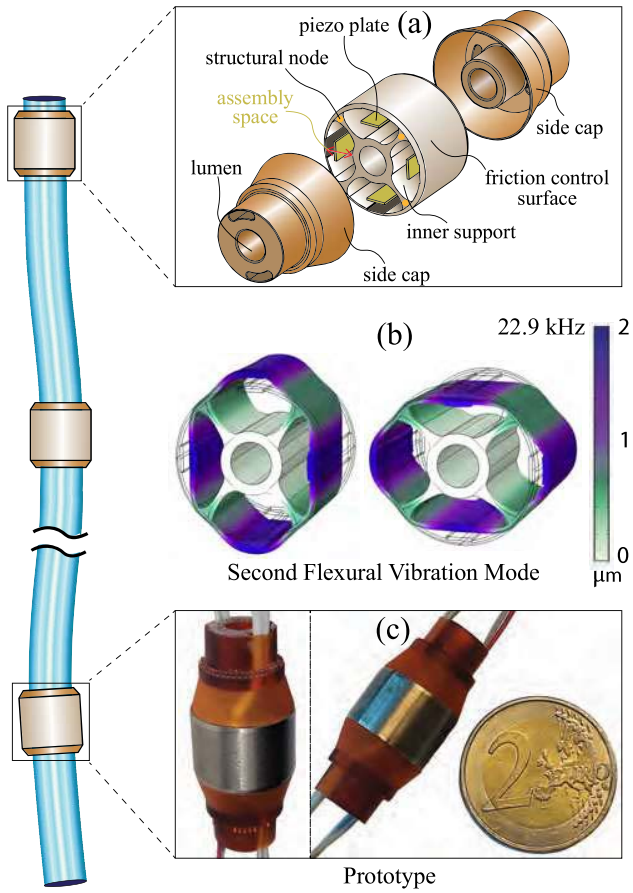

Fig. 2. Design, simulation and implementation of friction control modules. (a) shows the design of the friction control modules featuring a ring structure and two side caps. The ring structure encompasses four piezoelectric plates and an inner support structure attached to the outer surface at the nodal lines to minimize vibration interference. (b) shows the finite element simulation of the vibration mode of the designed ring structure. (c) shows the implemented scaled-up prototype of the designed resonating ring structure.

the fluid film. This overpressure causes the two objects to separate, as shown in Fig. 1(b), resulting in a controllable coefficient of friction—a phenomenon known as ultrasonic friction modulation or ultrasonic lubrication [10], [11]. The amount of separation is monotonically correlated to the vibration amplitude, enabling precise and controllable active lubrication at the interface [10].

Ultrasonic lubrication technology has demonstrated its effectiveness across various applications, particularly in scenarios where friction modulation is essential, such as in tactile interfaces [12], contactless manipulation [13] and squeeze-film bearings [14], [15]. Moreover, ultrasonic lubrication has proven its capability to function in submerged liquid environments [16] as effective as in air environments, showcasing its versatility to different operating conditions. The capacity of ultrasonic lubrication to seamlessly transition between high and low friction states in different environments suggests its potential to fulfill the evident need of active friction modulation in catheters.

B. Conceptual Design

Leveraging the concept of ultrasonic lubrication to actively control friction in catheters, we introduce a discrete module design concept in which friction control modules are integrated along the shaft of the catheter as shown in Fig. 2. The design requirements for the friction control modules, to ensure proper functionality, includes technology and application requirements. To be effective, the modules should achieve ($\geq$ 2 μm) of vibration amplitude at an ultrasonic frequency ($\geq$ 20 kHz) for maximal lubrication [17], [18]. The catheter application requires the design to be tubular, to have a lumen and to have the potential to be downsized. With these requirements in mind, we designed friction control module, illustrated in Fig. 2(a), which features a resonating ring structure and sealing side caps. The resonating ring encompasses a vibrating surface and an inner support structure with a lumen. The vibrating outer surface of the resonating ring comprises four piezoelectric plates, as shown in Fig. 2(a), such that when the piezoelectric plates are activated, a standing flexural wave is induced in the ring as depicted in Fig. 2(b). The frequency of this wave coincides with the second flexural resonance mode (second harmonic) of the ring structure, which is governed by the diameter and wall thickness of the ring. To properly support the ring, the inner support structure is connected to the ring at the nodal lines of the standing wave through thin walled Webs, as illustrated in Fig. 2(a). These Webs ensure minimal interference with the generated wave. The ring structure is sealed from both sides through the side caps, which insulates the piezoceramic plates chambers while featuring routing for the power wires. The wall of the side caps are designed to be flexible to not interfere with the ring vibrations.

C. Design and Simulation

We carried out a computational finite element method (FEM) simulation to estimate the resonant frequency and the potential

amplitude that this arrangement can reach. We first selected a scaled-up size for the concept with a diameter of 15 mm for ease of manufacturing. We built the model using COMSOL Mutliphysics® (COMSOL AB, Stockholm, Sweden) in which we carried out two types of studies. We first ran an eigenfrequency study to identify the resonant frequency corresponding to the desired vibration mode. Then we ran a frequency response study in which we simulate the behaviour of the ring structure when the piezoceramic plates are activated at a given frequency, which we use to estimate the vibration amplitude and mode shape. The simulation process iterated on the design parameters to find the combination that would result in an ultrasonic frequency and vibration amplitude that meets the design requirements. For the design parameters selected (titanium, diameter of 15 mm, wall thickness of 0.5 *mm*), we found the second flexural resonant frequency to be (22.9 kHz) and the amplitude to potentially reaching (2 μm), as shown in Fig. 2(b).

D. Prototype Development

We fabricated a scaled-up titanium ring prototype with a diameter of 15 mm, wall thickness of 0.5 *mm* and length of 10 mm using wire discharge machining. A set of four 1 W ceramic piezoelectric plates, 0.3 mm thick, were then cut into the right size and glued manually to the fabricated ring using a specially-designed wedge system to apply a uniform force along its length. Afterwards, the 0.5 mm power wires were soldered and routed through the assembled side caps. The exploded view of the prototype assembly is illustrated in Fig. 2(a).

III. Experiments

To validate the concept of the friction control modules and characterize its performance, we conducted two experiments. The first experiment aimed to characterize the vibration performance of the resonating ring. The second experiment aimed to validate the friction control modules capability to modulate friction on different type of surfaces.

‘

A. Vibration Characterization Experiment

In this characterization experiment, we measured the vibration response of the resonating ring to the voltage input using a single point laser doppler vibrometer (LDV) (OFV5000, Polytec GmbH, Baden-Württemberg, Germany). To be able to scan the whole surface of the ring, we affixed the ring to a servo motor to allow the ring to rotate while controlling the laser beam of the LDV using a dual axis galvanometer (ScannerMAX Saturn 5B, Edmund Optics Inc., NJ, U.S.A.), as shown in Fig. 3(a). The galvanometer scans the ring longitudinally while the servomotor scans the ring at different orientation angles. The control of the galvanometer, servo motor and the readings of the LDV was facilitated through data acquisition cards, controlled through a MATLAB interface.

To quantify the performance of the ring, we employed four key evaluation criteria: the resonant frequency, the maximum vibration amplitude, the vibration mode and the effective surface area. We define the effective area as the area in which the vibration amplitude reaches more than or equal to two microns, essential to fulfill the technology requirements. For this quantification, we do three different measurements; a frequency response measurement to quantify the resonant frequency, a voltage sweep measurement at the identified resonant frequency to quantify the maximum amplitude and a surface scanning of the ring to identify the resonance mode and quantify the effective surface area.

The experimental procedure initiated by collecting the frequency sweep at the central point of each of the four anti-nodal lines

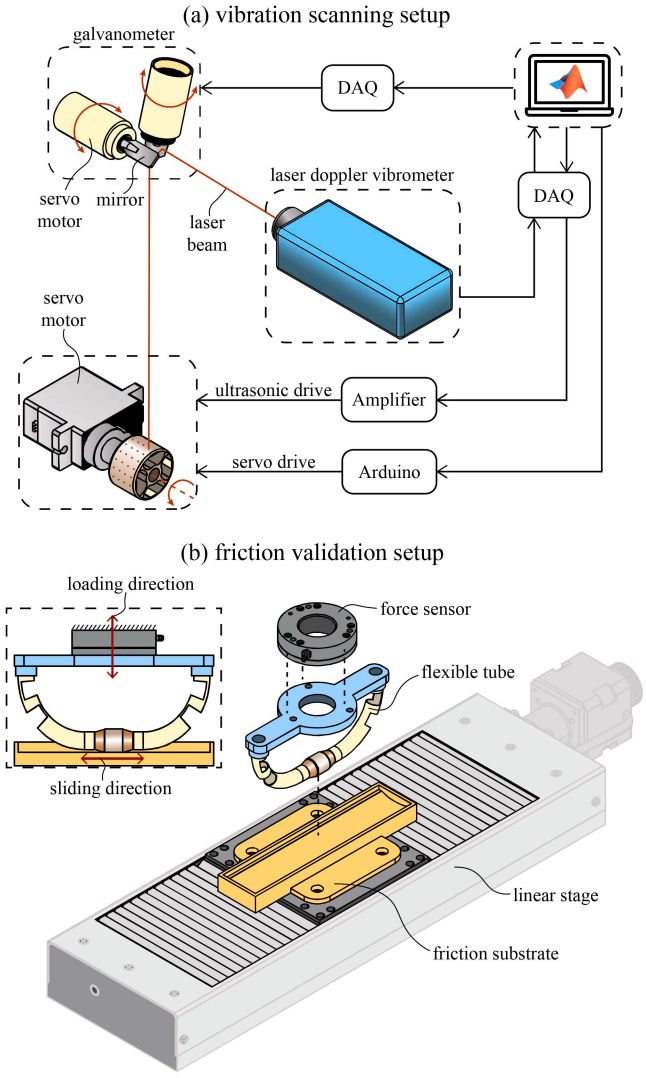

Fig. 3. Illustration of the experimental setups. (a) experimental setup to characterize the friction control module performance in terms of resonant frequency, maximum vibration amplitude, vibration mode and effective surface area. (b) experimental setup to validate the capacity of the friction control modules in modulating friction on soft and rigid substrates, representing healthy and calcified tissue, respectively.

followed by the voltage sweep at the identified resonant frequency. Afterwards, the surface scanning procedure started by positioning the ring at an anti-nodal line intersecting the laser beam path. Subsequently, we identified and discretized the measurable path into ten points longitudinally. The measurement algorithm then activated the transducers, concurrently recording responses at each designated point. Upon completion of one line scan, the ring underwent a 5-degree rotation, and the process iterated until a comprehensive response dataset around the ring was obtained.

B. Friction Validation Experiment

To validate the capacity of the friction control modules for modulating friction, we conducted sliding friction experiments on both rigid and soft surfaces. In this study, we secured the ring structure to a 6-axis force sensor (Nano43, ATI Industrial Automation, NC, U.S.A.) using a pair of flexible tubes to emulate the stiffness force of catheters. The module-sensor assembly was affixed to a manual linear slider to regulate the normal load. The friction substrates,

affixed opposite to the surface of the resonating ring, were allowed to slide against the ring surface using a motorized linear stage. Simultaneously, the LDV tracked the vibration amplitude from top of the resonating ring while sliding.

Friction experiments were conducted on two different friction substrates. The first one was a rigid 3D printed flat substrate using a rigid resin material (Model, FormLabs, MA, U.S.A.) with a post-cured elastic modulus of 2.3 GPa. The second substrate was a soft 3D printed flat substrate using a soft resin material (Elastic, FormLabs, MA, U.S.A.) with a post-cured ultimate tensile strength of 3.23 MPa and shore hardness of 50A. These two substrates represent the two ends of the mechanical properties spectrum in arteries: soft material representing healthy arteries and rigid material representing calcified arteries. Testing on both materials is essential because, while arteries are in principle soft, in reality, $>$ 70% of healthy individuals who are 40−49 years old suffer, to varying degrees, from coronary atherosclerosis [19], [20], [21], which involves the buildup of hard calcified plaque in arteries. Patients undergoing catheterization procedures already suffer from an advanced form of atherosclerosis, making it more likely for catheters to encounter calcified regions. This calcification stiffens the artery in general and more importantly on a local level, it forms rigid interface with catheters which was shown to have significantly higher coefficient of friction compared to healthy tissue [22]. Such a high friction with the calcified plaque can dis-integrate particles of the calcified plaque, leading to adverse consequences as they migrate through the bloodstream. Additionally, testing on rigid surfaces allows for comparing the performance of the proposed design to the existing devices in the benchmark application of haptic touchscreens [12], [17].

The experimental protocol began with loading the resonating ring on the friction substrate to (1 N), a critical load for catheters [23]. Then, the substrate started to slide at 1 mm/s for a distance of 15 mm. Two set of experimental data were collected. The first one was for a proof-of-concept test in which we activated the ultrasonic vibrations five seconds after sliding started, for a period of five seconds at a constant maximum vibration amplitude. In the second test, we activated a linearly modulated input voltage amplitude from a minimum to a maximum for a period of five seconds while sliding. Each sliding friction test was repeated six times.

To quantify the friction modulation capability, we use the friction reduction percentage, representing the amount of reduction in coefficient of friction as compared to the initial coefficient of friction before activating the vibrations, which can be calculated as follows:

$$\text{friction reduction } (\%) = \frac{|\mu_{off} - \mu_{on}|}{\mu_{off}} \tag{1}$$

IV. Results & Discussion

The experiments conducted to characterize the vibration of the resonating ring prototype unveiled a resonant frequency of approximately 20.5 kHz as shown in Fig. 4(a), slightly shifted from the frequency predicted from simulation. Additionally, we found the maximum vibration amplitude at the anti-nodal lines to be $\approx$ 3.2 μm, as shown in Fig.4(b), surpassing the predetermined amplitude of the design requirements. The observed variance between the experimentally identified resonant frequency and the simulation-predicted value can be attributed to discrepancies in the material properties between the predefined titanium alloy used in simulation and the actual alloy used to fabricate the prototypes. Additionally, the model assumes perfectly homogeneous material properties and does not account for the effects of machining processes and tolerances on the prototypes.

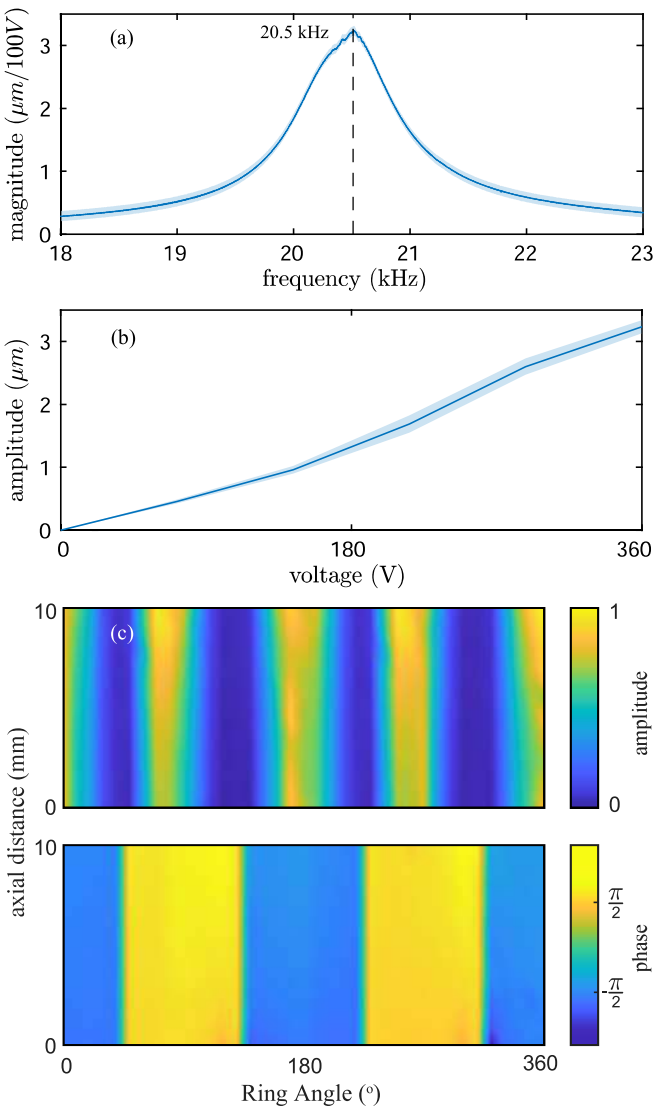

Fig. 4. Vibration characterization of the friction control module. (a) frequency response of the resonating ring along the anti-nodal lines. The solid line is the mean of the measurements across the four anti-nodal lines and the shade represents the standard deviation. (b) mapping between the input voltage and the output vibration amplitude along the anti-nodal lines. The solid line represents the mean of the measurements across the four anti-nodal lines and the shade represents the standard deviation. (c) vibration surface map of the resonating ring. The top color map represents the normalized vibration amplitude and the bottom shows the corresponding phase map. The measured surface map closely matches the anticipated vibration mode from simulation shown in Fig. 2(b), validating the design.

Upon scanning the surface of the resonating ring, at the identified resonant frequency, the corresponding mode was validated to be the second flexural mode as shown in Fig. 4(c), which closely matches the anticipated mode from simulation. The surface map further revealed that the active vibration surface of the resonating ring is approximately $\approx$ 50% of the entire surface of the resonating ring, implying that the friction modulation capability is limited to only half of the ring surface area. This relatively small active surface can be attributed to the rigid support connection at the nodal lines which limits the nodal line ability to rotate, thus limiting the vibration amplitude in the neighbouring areas.

The proof-of-concept friction experiment demonstrated the impact of activating the friction control module on the friction dynamics. Upon activating vibration, at the 5 second mark in Fig. 5(a), an

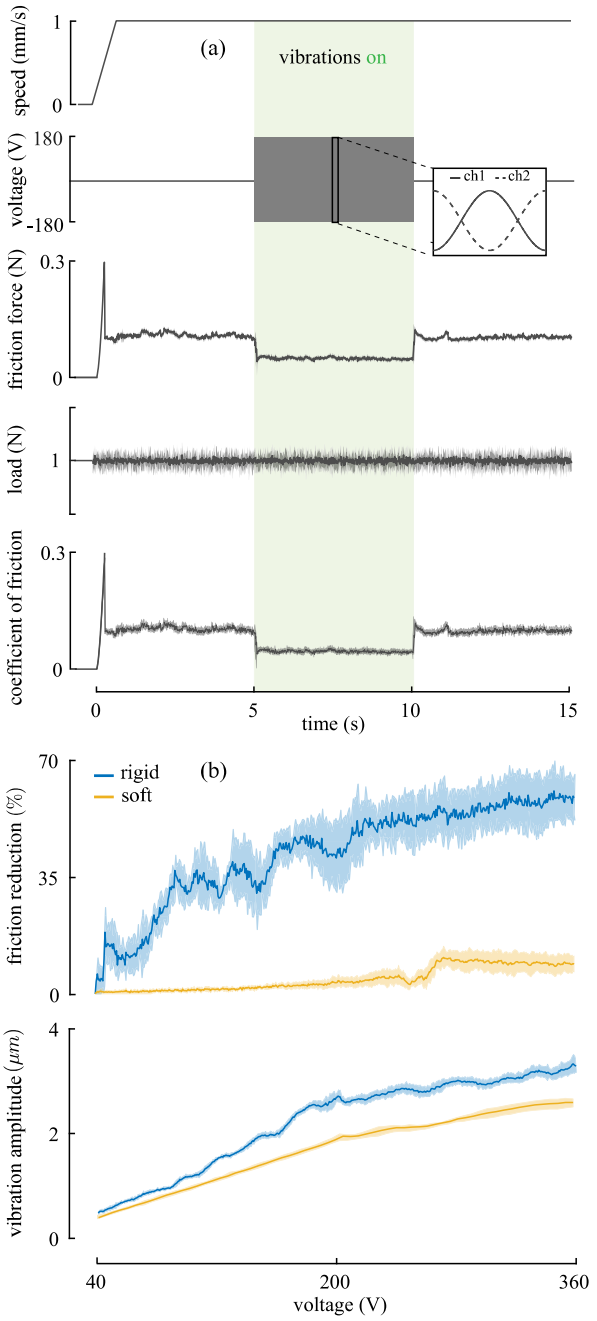

Fig. 5. Results of the friction validation experiments. (a) results of the proof-of-concept experiment which show that upon turning the vibrations on, both the friction force and the coefficient of friction decrease immediately by ≈ 60%, and revert promptly to its original state once vibrations are turned off. The observed behavior validate the impact of the proposed design for reducing friction. The solid lines represent the mean and the shadows represent the standard deviation of the repetitions. (b) results of the voltage modulation experiment on soft and rigid substrates, representing healthy and calcified tissue, respectively. In the rigid substrate case, the modulation of voltage modulated the vibration amplitude, resulting in linearly controllable friction, reaching up to ≈ 60% of friction reduction. In the soft substrate case, the voltage modulation similarly induce a modulation of the vibration amplitude. However, the friction reduction is only detectable at higher vibration amplitude, after which the reduction percentage follows a linear trend before saturating at ≈ 11%.

immediate reduction in both friction force and the coefficient of friction by ≈ 60% was observed. Subsequently, upon deactivation at the 10 second mark (Fig. 5(a)), the friction values reverted to their original state, confirming the friction control module ability to reduce friction. This demonstrated range of friction reduction matches the 60-80% typical friction reduction achieved by ultrasonic haptic touchscreens [12], [17], which serve as the benchmark for ultrasonic lubrication technology. This experiment was conducted on a flat surface interfacing with the curved surface of the friction control module, resulting in a line contact with very limited overlapping surface area. The overlapping surface area plays an important role in generating the desired lubrication effect, and despite it being limited, the module still exhibited significant friction reduction upon activation, showcasing its potential.

The voltage modulation friction experiment showed a corresponding modulation of the vibration amplitude, which in turn resulted in friction modulation at the interface as shown in Fig. 5(b). In the rigid case, the amount of friction reduction changes gradually across the entire input range reaching up to ≈ 60% reduction on average, showcasing the system ability not only to toggle between high and low friction states but also to finely control friction within this range. We observe a measurable friction reduction that only starts to appear at a certain vibration amplitude ≈ 0.6 μm. This value can be explained by the squeeze-film theory since a given amount of vibration amplitude is required to build sufficient pressure and be able to separate the two surfaces. We also observe that once the vibration amplitude exceeds the working threshold, the friction reduction percentage increases rapidly to the 35% level and afterwards it follows a linear trend towards the maximum reduction level. A possible explanation for the high sensitivity at the initial region can be that once the pressurized lubrication layer is formed, the disengagement of the asperities deep into the contact results in a high reduction gain. Once the shallow asperities are levitating, the system behaves more linearly.

Similarly, on the soft surface, modulating the voltage had a direct effect on the vibration amplitude. However, the friction reduction percentage appears to have significantly different dynamics as shown in Fig. 5(b). At first, we observe that no notable reduction in friction is achieved while the amplitude continues to increase up to ≈ 2 μm. Beyond this point, the reduction starts to increase linearly before rapidly saturating at ≈ 11% on average. This behaviour is well explained by the elasticity of the soft surface which, at the beginning, absorbs energy from the vibrating surface, preventing the lubrication layer from developing. Once vibration reaches a certain threshold, a separation between the two surfaces occurs and the lubrication layer can develop. The inherent elasticity, however, continues to play a role in limiting the pressure of the lubrication layer which thus causes the reduction to saturate.

It is important to note that the results obtained on the soft substrate may not accurately reflect what we would observe when testing on soft tissues, as these results are more specific to the damping properties of the soft material used in our tests. Previous research by Friesen et al. [24], [25] demonstrated that the damping factor of soft materials significantly affects the performance of ultrasonic lubrication. This significance of damping is because ultrasonic lubrication systems produce extremely low amplitudes, on the order of $O(10^1)$ μm, which results in minimal elastic effects, while vibration velocities are relatively large, on the order of $O(10^2)$ cm/s, leading to significant viscous damping effects. Moreover, Friesen et al. [24] found that materials with high damping factor is more favorable because its damping delays the response of the soft material to the source vibration, resulting in a phase shift between the vibration source and the soft surface. This phase shift allows a pressurized squeeze film to develop at the interface, leading to physical separation between the two surfaces and thus reduction in friction. Conversely, materials with low damping follow the vibration profile of the vibration source, preventing the squeeze

film from developing and thus resulting in no friction reduction. In their comparative experiment [25], they also found that human skin exhibited significantly higher damping compared to other common soft materials such as DragonSkin silicone rubber, similar to the material we used, indicating a potentially better response of actual soft tissues to ultrasonic lubrication.

One implicit assumption in our experiments is that contact occurs exclusively between the friction control modules and the friction substrate. While this is useful for assessing the performance of the friction control modules, in a real-world scenario, the main body of the catheter may also contact the blood vessel wall. Ideally, the modules should be slightly larger than the catheter's diameter to ensure that contact with the blood vessels occurs primarily with the friction control modules, minimizing contact with the catheter body itself. Thus, the size of the modules relative to the catheter diameter, as well as the distance between the modules, is crucial. Additionally, the catheter body should be coated with an ultra-low friction material to ensure smooth interaction with the blood vessel if contact occurs between the catheter body and the tissue. This ultra-low friction coating becomes feasible in this case since the friction control modules will provide stability when necessary by switching to their high-friction state.

One limitation of our current prototype is that the wires powering the piezoelectric actuators are routed through the lumen, obstructing it, and potentially limiting the catheter's functionality by reducing the available space for tool insertion. This issue can be addressed by embedding the wires within the catheter body, as demonstrated by Abdelaziz et al. [26], who developed a methodology to embed wires of various sizes and customized arrangements into the catheter body, enabling seamless power transmission throughout the catheter without compromising its functionality.

Other limitations of our current prototype are the difficulty to downsize and its limited lumen utilization, $\approx$ 20%, representing the lumen diameter compared to the overall module diameter. Both limitations arise from the need to maintain sufficient space between the piezoelectric plate and the inner support structure, illustrated as assembly space in Fig. 2(a), to facilitate the assembly of the plates. One potential solution is to have a separable inner support from the outer structure of the friction control module. This design would allow the inside of the module to be completely free during the assembly of the piezoelectric plates, providing more room for their installation. After assembly, the inner support could be inserted into place without requiring additional space for the assembly process, thereby maximizing lumen utilization post-assembly and enabling the possibility of downsizing. By designing this separable inner support to touch the nodal lines with needle-like edges, we could potentially also overcome the limitation of the small active vibratory area discussed earlier. This design would allow the nodal lines to rotate freely around the needle edges, unlike the rigid connection in the current design, thereby enhancing performance.

V. Conclusion & Future Work

We introduced a novel concept of a variable-friction catheter comprising discrete active resonating modules along its shaft. These modules use ultrasonic lubrication to actively control the coefficient of friction of its surface when in contact with the environment. We designed and implemented a scaled-up prototype of the friction control modules to validate our design. The experimental characterization showed that the implemented prototype fulfilled the technology requirements by successfully achieving $\approx$ 3.2 μm of vibration amplitude at an ultrasonic resonant frequency of 20.5 kHz. Vibrometry validated that the resonant mode matches that of the simulation and showed that the active vibratory surface area is $\approx$ 50% of the total surface area. Through sliding friction experiment, we validated that the modules can modulate friction on both soft and rigid substrates, representing soft and calcified tissue, with a maximum friction reduction percentage of $\approx$ 11% and $\approx$ 60%, respectively.

In the future, we plan to improve the miniaturization and to increase the active vibratory surface area. Both improvements are expected to lead to increased friction reduction particularly in scenarios where the modules are in contact with curved compliant interfaces. Moreover, we will investigate the effect of different parameters including the curvature of the sliding surface and the orientation of the friction control modules. Both parameters are key to understand the friction modulation phenomenon when the interfaces are curved. In addition, we plan to develop a waterproof design to allow for testing in liquid environments, a crucial aspect of the environment in which catheters operate. Furthermore, we plan to test the efficacy of the system in a clinically relevant environment on lubricated ex-vivo healthy and calcified tissue. Finally, we will assess the safety of the technology by capturing the thermal footprint of the friction control modules while in contact with tissue and examining the surface of tissue samples for potential damage.

Acknowledgment

The authors would like to thank Remi van Starkenburg, from the central workshop of TU Delft (DEMO), and Maurits Pfaff, from the Cognitive Robotics department at TU Delft, for their technical support in the fabrication of the prototypes.

References

[1] R. M. F. Wagner, R. Maiti, M. J. Carré, C. M. Perrault, P. C. Evans, and R. Lewis, "Bio-tribology of vascular devices: A review of tissue/device friction research,". *Biotribology*, vol. 25, Mar. 2021, Art. no. 100169.

[2] K. Takashima, R. Shimomura, T. Kitou, H. Terada, K. Yoshinaka, and K. Ikeuchi, "Contact and friction between catheter and blood vessel," *Tribol. Int.*, vol. 40, no. 2, pp. 319–328, 2007.

[3] Z. Wang, K. Wang, and Y. Xu, "Friction injury of the central vein caused by catheter for hemodialysis: An in vitro study," *Sci. Rep.*, vol. 14, p. 5836, Mar. 2024.

[4] M. Wilson, "Catheter lubrication and fixation: Interventions," *Brit. J. Nurs.*, vol. 22, no. 10, pp. 566–569, 2013.

[5] E. Brocchi, R. Pezzilli, P. Tomassetti, D. Campana, A. M. Morselli-Labate, and R. Corinaldesi, "Warm water or oil-assisted colonoscopy: Toward simpler examinations?" *Amer. J. Gastroenterol.*, vol. 103, no.3, pp. 581-587, 2008.

[6] A. Hernandez, R. Cogdill, C. Hinojosa-Laborde, and M. I. Restrepo, "Comparison of silicone spray versus water soluble lubricating jelly for the aid in bronchoscopic examination," *J. Anesthesiol. Clin. Sci.*, vol. 2, no. 7, pp. 1–5, 2013.

[7] J. Wang, L. Ma, W. Li, and Z. Zhou, "Influence of different lubricating fluids on friction trauma of small intestine during enteroscopy," *Tribol. Int.* vol. 126, pp. 29–38, Oct. 2018.

[8] P. Wyman, "Hydrophilic coatings for biomedical applications in and ex vivo," in *Coatings for Biomedical Applications*. Sawston, U.K.: Woodhead Publ., 2012, pp. 3–42.

[9] A. Niemczyk, M. El Fray, and S. E. Franklin, "Friction behaviour of hydrophilic lubricious coatings for medical device applications," *Tribol. Int.*, vol. 89, pp. 54–61, Sep. 2015.

[10] M. Wiertlewski, R. Fenton Friesen, and J. E. Colgate, "Partial squeeze film levitation modulates fingertip friction," *Proc. Nat. Acad. Sci. United States Amer.*, vol. 113, no. 33, pp. 9210–9215, 2016.

[11] R. F. Friesen, M. Wiertlewski, M. A. Peshkin, and J. E. Colgate, "The contribution of air to ultrasonic friction reduction," in *Proc. IEEE World Haptics Conf. (WHC)*, 2017, pp. 517–522.

[12] L. Winfield, J. Glassmire, J. E. Colgate, and M. Peshkin, "T-PaD: Tactile pattern display through variable friction reduction," in *Proc. 2nd Joint EuroHaptics Conf. Symp. Haptic Interfaces Virtual Environ. Teleoper. Syst.*, 2007, pp. 421–426.

[13] R. Gabai, R. Shaham, S. Davis, N. Cohen, and I. Bucher, "Contactless stage based on near-field acoustic levitation for object handling and positioning—Concept, design, modeling, and experiments," *IEEE/ASME Trans. Mechatronics*, vol. 24, no. 5, pp. 1954–1963, Oct. 2019.

[14] S. Zhao, S. Mojrzisch, and J. Wallaschek, "An ultrasonic levitation journal bearing able to control spindle center position," *Mech. Syst. Signal Process.*, vol. 36, no. 1, pp. 168–181, 2013. [Online]. Available: http://dx.doi.org/10.1016/j.ymssp.2012.05.006

[15] M. Shi, K. Feng, J. Hu, J. Zhu, and H. Cui, "Near-field acoustic levitation and applications to bearings: A critical review," *Int. J. Extreme Manuf.*, vol. 1, no. 3, 2019, Art. no. 32002.

[16] M. A. Atalla, R. A. J. Van Ostayen, A. Sakes, and M. Wiertlewski, "Incompressible squeeze-film levitation," *Appl. Phys. Lett.*, vol. 122, no. 24, 2023, Art. no. 241601. [Online]. Available: https://doi.org/10.1063/5.0149501

[17] M. Biet, F. Giraud, and B. Lemaire-Semail, "Squeeze film effect for the design of an ultrasonic tactile plate," *IEEE Trans. Ultrason., Ferroelectr., Freq. Control*, vol. 54, no. 12, pp. 2678–2688, Dec. 2007.

[18] T. Watanabe and S. Fukui, "A method for controlling tactile sensation of surface roughness using ultrasonic vibration," in *Proc. 1995 IEEE Int. Conf. Robot. Autom.*, 1995, pp. 1134–1139, doi: 10.1109/ROBOT.1995.525433.

[19] H. Mori, S. Torii, M. Kutyna, A. Sakamoto, A. V. Finn, and R. Virmani, "Coronary artery calcification and its progression: What does it really mean?" *JACC, Cardiovasc. Imag.*, vol. 11, no. 1, pp. 127–142, 2018.

[20] M. S. Kim et al., "Prevalence of coronary atherosclerosis in asymptomatic healthy subjects: An intravascular ultrasound study of donor hearts," *J. Atheroscler. Thromb.*, vol. 20, no. 5, pp. 465–471, 2013.

[21] E. M. Tuzcu, "High prevalence of coronary atherosclerosis in asymptomatic teenagers and young adults: Evidence from intravascular ultrasound," *Circulation*, vol. 103, no. 22, pp. 2705–2710, 2001.

[22] O. M. McGee, W. Sun, and L. M. McNamara "An in vitro model quantifying the effect of calcification on the tissue–stent interaction in a stenosed aortic root," *J. Biomechan.*, vol. 82, pp. 109–115, Jan. 2019.

[23] N. Xiao, J. Guo, S. Guo, and T. Tamiya, "A robotic catheter system with real-time force feedback and monitor," *Australas. Phys. Eng. Sci. Med.*, vol. 35, pp. 283–289, Sep. 2012.

[24] R. F. Friesen, M. Wiertlewski, and J. E. Colgate, "The role of damping in ultrasonic friction reduction," in *Proc. IEEE Haptics Symp. (HAPTICS)*, 2016, pp. 167–172.

[25] R. Fenton Friesen, M. Wiertlewski, M. A. Peshkin, and J. E. Colgate, "Bioinspired artificial fingertips that exhibit friction reduction when subjected to transverse ultrasonic vibrations," in *Proc. IEEE World Haptics Conf. (WHC)*, 2015, pp. 208–213.

[26] M. E. M. K. Abdelaziz et al., "Fiberbots: Robotic fibers for high-precision minimally invasive surgery," *Sci. Adv.*, vol. 10, no. 3, 2024, Art. no. eadj1984.